DNA Methylome Regulates Virulence and Metabolism in *Pseudomonas syringae*

Jiadai Huang[1#], Fang Chen[1#], Beifang Lu[1], Yue Sun[1], Youyue Li[1], Canfeng Hua[1], Xin Deng[1,2,3,4*]

[1] Department of Biomedical Sciences, City University of Hong Kong, 83 Tat Chee Rd, Kowloon Tong, Hong Kong, China

[2] Shenzhen Research Institute, City University of Hong Kong, Shenzhen, Guangdong, China

[3] Tung Research Centre, City University of Hong Kong, Hong Kong SAR, China

[4] Chengdu Research Institute, City University of Hong Kong, Chengdu, China

[*]To whom correspondence should be addressed: Dr. Xin Deng. Tel: +852 3442 5693; Fax: +852 3442 0549; E-mail: xindeng@cityu.edu.hk.

[#] These authors contributed equally to the paper as the first authors.

Abstract

Bacterial pathogens employ epigenetic mechanisms, including DNA methylation, to adapt to environmental changes, and these mechanisms play important roles in various biological processes. *Pseudomonas syringae* is a model phytopathogenic bacterium, but its methylome is less well known than that of other species. In this study, we conducted single-molecule real-time sequencing to profile the DNA methylation landscape in three model pathovars of *P. syringae*. We identified one Type-I restriction-modification system (HsdMSR), including the conserved sequence motif associated with N^6-methyladenine (6mA). About 25%–40% of the genes involved in DNA methylation were conserved in two or more of the strains, revealing the functional conservation of methylation in *P. syringae*. Subsequent transcriptomic analysis highlighted the involvement of HsdMSR in virulent and metabolic pathways, including the Type III secretion system, biofilm formation, and translational efficiency. The regulatory effect of HsdMSR on transcription was dependent on both strands being fully 6mA methylated. Overall, this work illustrated the methylation profile in *P. syringae* and the critical involvement of DNA methylation in regulating virulence and metabolism. Thus, this work contributes to a deeper understanding of epigenetic transcriptional control in *P. syringae* and related bacteria.

Keywords: *Pseudomonas syringae*, SMRT, DNA methylation, DNA methyltransferase, epigenetic

Introduction

Pseudomonas syringae inflicts leaf spots and cankers on plants globally, and its adequate control poses significant challenges. More than 60 pathovars have been identified, which infect almost all economically important crops in the world (1, 2). *P. syringae* pv. *phaseolicola* 1448A (*Psph*), one of the classical strains of *P. syringae*, can cause severe halo blight of common beans (*Phaseolus vulgaris*), which raises it from a common pathogen to a molecular plant-pathogen bacterium(3). *P. syringae* pv. *tomato* DC3000 (*Pst*) and *P. syringae* pv. *syringae* B728a (*Pss*) are two other model strains whose natural host plants are tomatoes and beans, respectively (4, 5). The most important weapon of *P. syringae,* and the first to be characterised, is the Type III secretion system (T3SS) encoded by *hrp* and *hrc* gene clusters, which are flanked by the conserved effector locus and deliver T3 effectors into host cells (6).

The expression of T3SS genes is inhibited in nutrient media such as King's B (KB), whereas it is induced in minimal medium or plant cells (7-9). The HrpRSL pathway is the primary regulator of the T3SS in *P. syringae*, with HrpRS activating *hrpL* expression. HrpL then binds to the *hrp* box to induce the translation of downstream T3 effectors (10-12). HrpRSL also impacts other virulence-related mechanisms, including motility, biofilm formation, siderophore production, and oxidative stress resistance, which are under the control of complicated regulatory networks, allowing *P. syringae* to infect plants (13-19). However, the methylome and function of DNA methylation in *P. syringae* pathogenesis and metabolism remain largely unknown.

In bacteria, DNA methylation is the primary level of epigenetic regulation because

59 these prokaryotes lack the histones and nucleosomes of eukaryotic cells. Bacterial
60 DNA has three primary forms of methylation: N^6-methyladenine (6mA), N^4-
61 methylcytosine (4mC), and N^5-methylcytosine (5mC). The latter is the most common
62 type in eukaryotes, while 6mA is the dominant form in prokaryotes. DNA methylation
63 in bacteria is mainly the product of methyltransferase (MTase) enzymes, which
64 transfer a methyl group from S-adenosyl-l-methionine to various positions on target
65 bases, depending on the modification (20). MTases originate from the restriction-
66 modification (R-M) system, which protects bacterial cells from invading DNA by
67 recognising and cleaving specific unmethylated motifs (21, 22). There are three main
68 types of R-M systems, Types I, II, and III, categorised according to the related
69 subunits and the precise site of DNA restriction (23, 24). Additionally, orphan MTases
70 are an emerging group of MTases without cognate restriction that are involved in the
71 regulation of DNA replication and gene expression (21). The Type I R-M system
72 contains three host-specificity determinant (*hsd*) subunits, restriction (R),
73 modification (M), and specificity (S), which are encoded by *hsdR*, *hsdM*, and *hsdS*,
74 respectively. Genome sequencing and bioinformatics analyses have revealed that the
75 HsdMSR system exists in around half of all bacteria and archaea species (24).
76 Nonetheless, the biological roles and specific motifs alongside their targets of most
77 MTases remain unknown, especially those related to 6mA (25).
78 A new sequencing technology, single-molecule real-time (SMRT) sequencing, can
79 detect all three forms of DNA methylation, but particularly 6mA (26). SMRT-seq has
80 been applied for complete genome sequencing and insertion sequence profiling in

81 different *P. syringae* pv. *actinidiae* (*Psa*) strains (27-29). In *P. aeruginosa*, Type I R-M
82 systems, along with their specific motifs, have been identified in the model strain
83 PAO1 and two clinical strains via SMRT-seq. These MTases are considered to play
84 important roles in *P. aeruginosa* virulence or drug resistance (30-32).
85 To study the targets and functions of DNA modifications in *P. syringae*, SMRT-seq
86 was used to identify global methylation sites and reveal their conserved and divergent
87 functions in the three model strains in this study. We found that HsdMSR in *Psph* was
88 involved in modulating three pathways, namely T3SS, biofilm production, and the
89 metabolism-related gene expression of ribosomal proteins. Moreover, we found that
90 HsdMSR-mediated transcriptional regulation depends on the full methylation of both
91 DNA strands. Taken together, our results provide insights into the involvement of
92 DNA methylation in the phenotypic traits of *P. syringae* and transcription regulatory
93 mechanisms that may apply to other pathogenic bacteria.

94 **Results**

95 **Genome-wide methylome profiling of three model *P. syringae* strains**

96 According to REBASE (33) database prediction, 0 to 2 Type I R-M systems and 3 to 4
97 Type II R-M systems exist in the three pathovars of *P. syringae*, indicating that Type I
98 is more conserved than Type II in this pathogen **(Table S1)**. To characterise their
99 methylomes, we performed SMRT-seq to obtain the methylation patterns on a
100 genome-wide scale using DNA extracted from the stationary phase of the three wild-
101 type (WT) strains. Our results revealed a total of 10,302 modified bases, of which
102 3,849, 4,646, and 1,807 nucleotides were significantly identified as being 6mA, 5mC,
103 and 4mC modified, with an interpulse duration ratio (IPD) of > 1.5 throughout the
104 genome of *Psph* **(Fig. 1A)**. After identifying the significantly modified sites, we
105 orientated the gene locus tags within the methylated bases. Most genes harboured
106 only 6mA modifications, although 339 genes harboured all three DNA methylation
107 types **(Fig. 1B)**.

108 In *Pst*, a total of 6,002, 2,242, and 3,514 methylation sites were significantly
109 identified as 6mA, 4mC, and 5mC, respectively, using the same cut-off (IPD >1.5)
110 **(Fig. 1C)**. Among these modified bases, a higher degree of overlap was observed
111 across all three types of methylation than in *Psph*, with 591 (17.7%) genes exhibiting
112 modifications in their sequences **(Fig. 1D)**. Additionally, the methylome atlas of *Pss*
113 revealed a lower incidence of methylation than those of *Psph* and *Pst*, particularly in
114 terms of 6mA modifications, which were only seen in 457 significant occurrences
115 **(Fig. 1E)**. Comparative analysis of the three methylations in *Pss* showed that the

116 highest numbers of genes were modified by 4mC and 5mC simultaneously (**Fig. 1F**).

117

118 **Characteristics of modification loci and GC contents in *P. syringae***

119 To further uncover the distribution of the modifications throughout the genome, we
120 calculated how many of the three kinds of modification sites were in these three
121 strains. The majority of modifications occurred in coding sequence (CDS) regions,
122 accounting for at least 80% **(Fig. S1A)**, and less than 20% were in intergenic regions
123 and non-coding RNA (tRNA and rRNA). However, compared with 4mC and 5mC,
124 6mA was more likely to be in intergenic regions, which suggests that it potentially
125 functions in transcription regulation in *P. syringae*.

126 It is known that 5mC occurs within CpG sites in CpG islands, which contain higher
127 GC percentages than is typical in the human genome (34). Additionally, the GC
128 architecture can influence DNA methylation in eukaryotic cells (35). To determine the
129 GC content characteristics of modification sites in *P. syringae*, we extracted the
130 sequences 50-bp upstream and downstream from the modified bases and calculated
131 their GC content. The distribution of modification sites and their GC content are
132 shown in density plots. Compared with 4mC and 5mC, the GC contents of 6mA sites
133 were the lowest and the closest to the average GC percentage of *P. syringae* (58% for
134 *Psph* and *Pst*, 59.2% for *Pss*) **(Fig. S1B)**. In contrast, 5mC modification bases had the
135 highest GC content, especially in *Pss* **(Fig. S1C)**. Furthermore, 4mC sites in *Psph* had
136 a higher GC content than those in *Psa* and *Pss* **(Fig. S1D)**. Similar phenomena have
137 been observed in various other bacterial species. For instance, the *Escherichia coli*

138 MTase Dcm can catalyse the 5′CCWGG3′ motif (36). Furthermore, in *Spiroplasma* sp.
139 strain MQ-1, more than 95% of 5mC modifications are found in high-CG sequences,
140 which is similar to the pattern in eukaryotes (37).
141

142 **Methylated genes revealed highly functional conservation among three *P.***
143 ***syringae* strains**

144 When we compared the three methylation types in the three tested strains, we noticed
145 different levels of similarity among them **(Fig. 2A-B and Table S2)**. Notably, about
146 25% to 45% of methylated genes were conserved in more than two of the strains.
147 Interestingly, 5mC had the highest conservation level (39.1%), which might be
148 explained by the rare occurrence of 6mA in *Pss*. Conversely, an obviously higher
149 degree of conservation was observed in virulence-related genes, including T3SS and
150 alginate biosynthesis-related genes, between *Psph* and *Pst* **(Table S2)**. Additionally,
151 some methylated genes (n = 739) harboured sites for different modification types in
152 the three strains **(Fig. 2A)**. For example, the modification sites of a Cro/CI family
153 transcriptional factor (TF) in PSPPH_1319 were for different modification types in
154 the three *P. syringae* strains. *Psph* carried 6mA and 5mC, while *Pst* and *Pss* had 5mC
155 and 4mC. This difference might result from differences in the MTases and their
156 specific motifs **(Table S2)**.

157 To elucidate the functions of genes methylated with these three modification types,
158 functional enrichment analyses were performed based on gene ontology (GO) and
159 Kyoto Encyclopedia of Genes and Genomes (KEGG) databases (38, 39). Analysis

160 revealed the shared functional characteristics of genes with 5mC and 4mC
161 modifications in *Pss* and *Pst*. In contrast, genes with 6mA modifications exhibited
162 greater conservation between *Psph* and *Pst* **(Fig. 2C)**. For instance, *Pst* and *Pss*
163 contained 4mC-methylated genes enriched in signalling transduction and TF binding,
164 whereas *Psph* exhibited enrichment in oxidation–reduction process and nucleic acid
165 binding genes. Remarkably, significant conservation of functional terms was observed
166 for genes with 6mA modifications, with at least 21 terms conserved between *Psph* and
167 *Pst*. These terms included ATP binding, catalytic activity, integral component of
168 membrane, transferase activity, and phosphorylation. We also conducted Cluster of
169 Orthologous Group (COG) protein function analysis (40, 41), which assigned the
170 methylated genes from the three strains to 20 categories with diverse functions **(Fig.**
171 **S2A-C)**. In *Psph*, the top three COG classifications encompassed inorganic ion
172 transport, amino acid transport, and transcription **(Fig. S2A)**. Furthermore, the
173 abundance of modified genes related to cell wall/membrane/envelope biogenesis (M
174 category) in *Pss* was lower than that of *Psph* and *Pst*. Despite the slight variations in
175 COG distribution, the overall pattern exhibited considerable similarity and
176 conservation across the three strains.
177

178 **Five conserved sequence motifs of 6mA and 4mC were identified in *P. syringae***

179 Obtaining the whole methylomes of the three strains led us to investigate the
180 associated MTases and their target motifs. The PacBio motif finder and MEME suite
181 (42) were used to determine the specific sequence motifs within 50 bp upstream and

182 downstream of the significantly modified bases. Using the results of both software
183 packages with corresponding cut-offs, we identified two 6mA motifs in *Psph:*
184 C**A**GCN$_{(6)}$CTC and RAGT**A**CTY **(Fig. 3A)**. The bolded bases indicate the
185 methylation sites in these motifs. The two motifs occurred a total of 2,998 and 300
186 times in double strands, and more than 98% and 77% of those occurrences were
187 methylated, respectively, revealing the high methylation rates of these two motifs and
188 implying their crucial roles in *Psph* **(Fig. 3B)**. However, the analysis did not identify
189 any credible motifs for cytosine modifications.
190 Three motifs for 6mA and one motif for 4mC were identified in *Pst* **(Fig. 3C)**. The
191 first 6mA motif, CAARG**A**A, was found 2,022 times in the genome, with 2,019 of the
192 occurrences methylated (99.8%) **(Fig. 3D)**. The second 6mA motif, G**A**AN$_{(4)}$RTRCC,
193 was fully methylated in both strands. Similarly, the last 6mA motif, GY**A**GN$_{(5)}$CTRC,
194 exhibited a high methylation level (96%) in the genome of *Pst*. Conversely, the only
195 motif identified for 4mC in *Pst* displayed a considerably lower methylation level than
196 the 6mA sites, with 2,207 occurrences of methylation out of a total of 8,048 sites
197 (approximately 27%). Notably, no credible motifs were found in *Pss* because of its
198 noticeably lower modification levels compared with the other two strains. Overall, the
199 application of SMRT-seq to the three model *P. syringae* strains identified specific
200 sequence motifs, including 6mA motifs, exhibiting extensive methylation statuses.
201
202 ***In vivo* validation revealed the activity and specificity of Type I R-M system**
203 **MTase in *Psph***

204 The first motif, C**A**GCN$_{(6)}$CTC, identified in *Psph* is similar to the counterpart
205 modified by a Type I R-M MTase in *P. aeruginosa* (26) **(Fig. S3)**, suggesting that the
206 putative HsdMSR is responsible for the observed motif. As no other motifs exhibited
207 a discernible association with the Type II R-M MTases, we opted to focus our
208 investigation on the putative HsdMSR in *Psph.* To determine the potential functions
209 of the putative MTases, we constructed MTase knock-out mutants and complementary
210 strains of HsdMSR. Growth curve experiments showed the adverse effects on
211 Δ*hsdMSR* compared to the WT strain **(Fig. S4)**.
212 In accordance with previous studies showing that growth conditions affect the
213 bacterial methylation status, we applied dot blot experiments to detect the 6mA levels
214 of *Psph* in the logarithmic and stationary phases. The results revealed that 6mA levels
215 in the stationary phase were much higher than those in the logarithmic phase **(Fig.**
216 **S5A)**. To confirm the activity of HsdMSR, a dot blot assay was used to detect the
217 6mA intensity in WT and Δ*hsdMSR*. The results shown in **Fig. S5B** illustrate that
218 6mA levels were significantly decreased in Δ*hsdMSR* compared to the WT, but were
219 restored in the complemented strain. In addition, SMRT-seq was performed on
220 Δ*hsdMSR*, which further confirmed that HsdMSR and its specificity were crucial for
221 maintaining methylation levels in *P. syringae*. Δ*hsdMSR* lacked all the 6mA sites
222 within the identified C**A**GCN$_{(6)}$CTC motif found in the WT **(Fig. S5C)**. Taken
223 together, the results demonstrated that 6mA levels change with the bacterial growth
224 phase, and HsdMSR is responsible for maintaining 6mA sites within the sequence
225 motif of C**A**GCN$_{(6)}$CTC.

226

227 **Transcriptomic analysis profiling of differentially regulated genes associated**
228 **with virulence and metabolism in the HsdMSR mutant**

229 To explore the regulatory influence of HsdMSR on gene expression, RNA-seq was
230 applied to analyse WT and Δ*hsdMSR* in the stationary growth phase, which ensured
231 that the strains had sufficient DNA methylation levels. Differentially expressed genes
232 (DEGs) were obtained with the cut-off of $|\log_2 FC| > 1$ and an adjusted p-value < 0.05.
233 We identified 395 DEGs between WT and Δ*hsdMSR* under these experimental
234 conditions. Among these, 218 genes were upregulated, while 177 genes were
235 downregulated compared with the WT **(Fig. 4A and Table S3)**. To investigate the
236 functional differences between WT and Δ*hsdMSR*, GO and KEGG databases were
237 used to perform functional enrichment analyses based on the DEGs. When using
238 adjusted p-value < 0.05 as a significant cut-off, the upregulated functional terms
239 included alginate biosynthesis, fructose and mannose metabolism, and the oxidation–
240 reduction process **(Fig. 4B)**. The downregulated pathways included the citrate cycle,
241 oxidative phosphorylation, ribosome structure, and translation **(Fig. 4B)**.

242 We also analysed the function alteration via COG category analysis of DEGs, which
243 revealed that the upregulated genes were more likely to be involved in lanes E (amino
244 acid transport and metabolism), G (carbohydrate transport and metabolism), and I
245 (lipid transport and metabolism) **(Fig. 4C)**. Downregulated DEGs were significantly
246 involved in lanes F (nucleotide transport and metabolism) and J (translation,
247 ribosomal structure, and biogenesis) **(Fig. 4D)**. To investigate the correlation between

248 DEGs and HsdM-recognising motif sites, we performed comparative analysis to
249 reveal 76 genes that overlapped **(Fig. 4E)**. Eight DEGs harboured the HsdMSR
250 methylation motif at the putative promoter region (within 100-bp upstream of the
251 gene) **(Table S4)**.
252
253 **HsdMSR was required for T3SS and biofilm formation in *P. syringae***
254 To confirm the RNA-seq results, we performed quantitative real-time PCR (RT-qPCR)
255 experiments on T3SS genes. Several T3SS effector genes were identified as
256 upregulated, including *hopAE1*, *hrpF*, *hrpA2*, *hrpK1*, and *hrpW1*. RT-qPCR was
257 applied under the same conditions as RNA-seq, and the transcriptional levels of all
258 genes were confirmed as being significantly higher in the Δ*hsdMSR* than the WT **(Fig.
259 5A)**. These gene expression levels were restored in the complemented strain. To
260 determine whether the loss of HsdMSR affected the *Psph* virulence phenotypes
261 because of alterations to T3 effectors, we allowed the WT, Δ*hsdMSR*, and
262 complemented strains to infiltrate the primary leaves of bean plants. At 6 days post-
263 inoculation, Δ*hsdMSR* was observed to induce more severe symptoms than the WT
264 and complemented strains **(Fig. 5B)**. Overall, HsdMSR inhibited the expression of T3
265 effectors under KB conditions, and the loss of this modification system enhanced the
266 pathogenicity of the strain during plant infection.
267 Besides T3SS, alginate biosynthesis-related genes were also observed among the
268 DEGs between WT and Δ*hsdMSR*. Alginate biosynthesis proteins have been
269 demonstrated to be essential for Extracellular polymeric substances (EPS) production,

270 which enhances biofilm formation during the bacterial infection process (43, 44). RT-
271 qPCR experiments were performed on the relevant genes, including *alg8*, *algE*, *alg44*,
272 *algF*, and *algD*. The expression levels of these genes in Δ*hsdMSR* were significantly
273 increased compared with the WT and complemented strain **(Fig. 5C)**. To further
274 investigate the influence of HsdMSR on biofilm formation, we performed a crystal
275 violet staining assay to detect biofilm production by the three strains. The intensity of
276 crystal violet staining of biofilms formed by the WT and complemented strains was
277 significantly less strong than that of Δ*hsdMSR* cells **(Fig. 5D)**, supporting the role of
278 HsdMSR in controlling biofilm formation. We therefore concluded that HsdMSR
279 regulates the virulence of *P. syringae* by tuning its expression of T3SS and alginate
280 biosynthesis genes.
281
282 **HsdMSR regulated ribosomal protein synthesis and translational efficiency**
283 We noticed that HsdMSR was important for bacterial growth **(Fig. S4)**, while the
284 expression of many ribosomal protein genes was reduced with the deletion of *hsdMSR*
285 **(Fig. 5E)**. Regulation of ribosomal gene expression is essential to the integrity of the
286 ribosome structure, which affects translation (45). Therefore, we hypothesised that the
287 low expression level of ribosome proteins in Δ*hsdMSR* would result in delayed
288 growth. We selected four genes encoding different ribosome subunits (*rplS*, *rpmD*,
289 *rpsS,* and *rpsJ*) to verify the RNA-seq results through RT-qPCR. While *rplS* and
290 *rpmD* encode 50S ribosomal proteins (L19 and L30), *rpsS* and *rpsJ* are responsible
291 for 30S ribosomal proteins (S19 and S10). The RT-qPCR results demonstrated that the

292 mRNA expression levels of these genes were significantly lower in Δ*hsdMSR* than in
293 WT, while levels in the complemented strain were restored to the WT level **(Fig. 5E)**.
294 Given the important role of ribosomal proteins in translation, we performed ribosome
295 profiling, also termed Ribo-seq, of the *Psph* WT and Δ*hsdMSR* strains to detect the
296 influence of HsdMSR on translational efficiency (TE). When we compared the WT
297 and Δ*hsdMSR*, the TE of 162 genes was significantly different ($|\log_2 FC| > 1.5$) (**Fig.
298 5F**). Of these genes, 73 genes had enhanced TE, while 89 had supressed TE (**Fig. 5F**).
299 Most of these genes were related to transmembrane transport and transcription
300 regulation **(Fig. S6A-B)**. Remarkably, the TE of genes linked to the oxidation-
301 reduction process tended to be supressed **(Fig. S6B)**. These results showed that
302 HsdMSR plays an important role in the regulation of metabolism by promoting
303 ribosomal protein synthesis and modulating TE in *Psph*.
304

305 **HsdMSR regulation of *hrpF* was dependent on the full methylation of both
306 strands**

307 To investigate whether and how HsdMSR directly affects gene expression, we
308 focused on those DEGs whose upstream regions harbour its motif. Interestingly, we
309 noticed a methylation motif in the upstream region of *hrpF* (encoding the
310 pathogenicity factor HrpF), which increased its expression level in the *Psph* WT strain
311 **(Fig. 5A and 6A)**. To further explore the effects of HsdMSR on the transcription of
312 *hrpF*, we constructed a *lux*-reporter plasmid carrying the motif and extended it by 50
313 bp, which covered the upstream region of *hrpF*. After transferring the plasmid into the

314 WT and Δ*hsdMSR* strains, we detected a significant difference in the expression level
315 of *hrpF-lux* between these two strains **(Fig. 6B)**. The *hrpF-lux* signal in Δ*hsdMSR*
316 increased along with culture time and reached a peak at 24 hours, when the
317 methylation level was also elevated in the late growth stage **(Fig. 6C)**. This result of
318 the *lux*-reporter assay confirmed the RNA-seq and RT-qPCR results showing that
319 *hrpF* was remarkably upregulated in Δ*hsdMSR* compared with the WT strain.
320 To detect the influence of the 6mA site within the HsdMSR motif on the expression of
321 *hrpF*, we induced a point mutation on the sense strand in the reporter plasmid to
322 change the 6mA to C (C**C**GCN$_6$CTC). This resulted in a low *hrpF* expression level
323 similar to that of the WT sequence carrying the A base **(Fig. 6D)**, indicating that a
324 hemi-methylated pattern is insufficient for transcriptional alteration. To verify our
325 hypothesis, we constructed a reporter with two A mutations (C**C**GCN$_6$C**G**C),
326 transferred it to the WT and Δ*hsdMSR* strains, and detected signal changes. As
327 expected, the reporter carrying the HsdMSR motif without two A bases resulted in a
328 significantly higher signal than the hemi-mutated and non-mutated reporters in the
329 WT **(Fig. 6E)**. Taken together, the results showed that HsdMSR regulation of *hrpF*
330 transcription was based on both strands being fully methylated.
331

332 **Discussion**

333 Recent advances in sequencing technology have expanded our understanding of DNA
334 methylation in bacteria. Numerous DNA MTases have been extensively characterised
335 in different pathogenic bacteria, and data on their distribution patterns, recognition
336 motifs, and biological functions have been collated (31, 32, 46-49). However, most
337 research has concentrated on animal pathogenic bacteria, with limited insights into
338 phytopathogenic bacteria except for *Xanthomonas*(50-52). Consequently, in this study,
339 we employed SMRT-seq to profile the methylome patterns and specific conserved
340 sequence motifs of three *P. syringae* strains. Notably, we discovered that the virulence
341 and metabolism of *Psph* are regulated by Type I R-M MTase HsdM. The
342 nonfunctional nature of the subunit restriction endonuclease HsdR was acknowledged,
343 although its potential functionality relies on the presence of MTase (30).

344 Comprehensive analysis of the methylome atlas revealed that 6mA is the most
345 prevalent modification type in *Psph* and *Pst*, mirroring the trends observed in other
346 bacteria. Conversely, *Pss* displays the lowest occurrences of 6mA throughout its
347 genome **(Fig. 1)**. This discrepancy might be attributed to the absence of the Type I R-
348 M MTase responsible for 6mA in *Pss*. Similarly, the presence of two Type I R-M
349 MTases in *Pst* possibly contribute to it having a higher number of 6mA sites than
350 *Psph*. Additionally, all three pathovars had a similar pattern, with 4mC being the least
351 frequent modification type. Despite belonging to the same *P. syringae* species, the
352 three strains tested displayed remarkably divergent methylation patterns, which is
353 reminiscent of the phenomenon observed in *Xanthomonas* spp. (50).

354 We further identified two (both 6mA) and four (three 6mA, one 4mC) motifs in *Psph*
355 and *Pst*, respectively, but none in *Pss* **(Fig. 3)**. In fact, more motifs were predicted by
356 the MEME and PacBio motif finders, but we chose only those motifs identified by
357 both algorithms for higher accuracy. We found that the 6mA motifs had extremely
358 high methylation levels, ranging from 77% to 100%, in the stationary phase of *P.*
359 *syringae*. We subsequently found that the 6mA methylation levels increased during
360 *Psph* growth, similar to the observations in *P. aeruginosa* (30). However, DNA
361 methylation is much more stable under different conditions and growth phases in
362 *Helicobacter pylori* and *Salmonella typhimurium* (53, 54).
363 MTases have been reported to play important roles in bacterial growth; for example,
364 they are involved in cell cycle processes such as chromosomal replication in *E. coli*
365 and *Caulobacter crescentus* (55-57). DNA methylation can activate DnaA and signal
366 the initiation of chromosome replication to affect the growth of gamma-proteobacteria
367 (58, 59). Previous studies revealed that DNA methylation influences bacterial growth
368 through genes related to diverse carbohydrate transport mechanisms (51). We report
369 that the 6mA modification catalysed by HsdM in *Psph* positively affects its growth,
370 which can be explained by the downregulation of ribosomal proteins and the
371 alteration of metabolism-related gene TE. However, many MTases are thought to be
372 uncorrelated to growth in bacterial species such as *P. aeruginosa* and *Klebsiella*
373 *pneumoniae* (30, 31, 48).
374 Many MTases and DNA methylations are involved in bacterial virulence through their
375 modulation of gene expression (30, 31, 48, 49, 51, 52, 60-62). In this study, RNA-seq

376 analysis of the HsdMSR mutation strain revealed 395 DEGs. Remarkably, not all
377 DEGs harboured the HsdMSR methylation motif in their promoter region. There were
378 no significant correlations between the HsdM-recognised motif sites in the promoter
379 region and DEGs, even though DNA methylation is generally known to affect gene
380 expression by altering the interactions between DNA and proteins such as TFs, which
381 compete with MTases at specific motif sites and thus influence downstream
382 transcription (63). However, recent studies have revealed that DNA methylation
383 within CDS can also alter gene expression in bacteria; for example, 5mC in CDS can
384 enhance transcription while blocking the transcription of CpG islands in promoters in
385 eukaryotic cells (64, 65). We hypothesise that 6mA in *Psph* can regulate gene
386 expression directly and indirectly. We confirmed that the 6mA motif in the promoter
387 region of *hrpF* can directly and negatively regulate gene transcription in a manner
388 dependent on full methylation of the strands **(Fig. 6)**. In addition, DNA methylation
389 can change DNA curvature to decrease the thermodynamic stability of the double
390 helix (66). Therefore, those DEGs carrying modified sites, including alginate
391 biosynthesis-related genes and T3 effectors, are believed to be caused by the alteration
392 of nucleoid topology, as seen in *Salmonella* and *H. pylori* (49, 67). Furthermore, the
393 6mA sites, including those in virulence-related *hrc/hrp* and *alg* genes, are conserved
394 in *Psph* and *Pst*, implying that similar phenotypes occur in the latter strain. Altogether,
395 6mA modifications in *Psph* were observed to act as important epigenetic regulators of
396 gene expression.
397 *P. syringae* uses its diverse abilities to infect plants. TFs play important roles in

398 virulence regulation and participate in sensory crosstalk by sensing environmental
399 signals and responding. Previous studies have illustrated these complex networks of
400 TFs in *P. syringae* (16, 18, 68) ; however, the degree to which genes are regulated at
401 the epigenetic level remains unknown. Here, we have provided novel insights into the
402 roles of 6mA in virulence-related gene regulation in *Psph*.
403 As more studies apply SMRT-seq to investigate bacterial methylomes, it has become
404 evident that the epigenetic regulation of gene expression is highly prevalent among
405 bacteria. Understanding the mechanisms through which methylation functions can
406 provide novel insights into how strain-specific epigenetic modifications shape the
407 adaptive responses of bacteria to distinct environmental challenges. As the repertoire
408 of MTases varies among *P. syringae* strains, this approach will help us to better
409 understand the diversity of DNA methylation and epigenetic patterns among *P.*
410 *syringae* species.
411

412 **Materials and methods**

413 **Bacterial strains and culture conditions**

414 The bacterial strains, plasmids, and primers used in this study can be found in **Table**
415 **S5**. All three model strains and mutations were cultured at 28 ℃ in KB medium with
416 shaking at 220 rpm or LB agar plates. The *E. coli* strains were grown at 37 ℃ in LB
417 broth (Luria-Bertani) with shaking at 220 rpm or on LB agar plates. Antibiotics were
418 used at the following concentrations: kanamycin at 50 μg/mL, spectinomycin at 50
419 μg/mL, and rifampin 25 μg/mL.

420 **DNA extraction and SMRT sequencing.**

421 Three WT model strains and HsdMSR knockout *Psph* strains were cultured to the
422 stationary phase. The genomic DNA of the strains was extracted using a TIANamp
423 Bacteria DNA kit (Tiangen Biotech), using the manufacturer's standard protocols. The
424 SMRT sequence was performed at Abace Biotechnology company using Pacific
425 Biosciences sequel II and Ile sequencer (PacBio, Menlo Park, CA, USA). SMRT-seq
426 reads were aligned to the genome reference of *Psph* 1448A (GCF_000012205.1), *Pst*
427 DC3000 (GCF_000007805.1), and *Pss* B728a (GCF_000012245.1), respectively.
428 SMRTLink software v13.0 was used to perform DNA methylation analysis. A
429 modification quality value (QV) score of 50 and 100 was used to call the modified
430 bases A and C, respectively.

431 **Deletion mutant and complemented strains construction**

432 The restriction enzymes digested the pK18mobsacB suicide plasmid(69) listed in
433 **Table S5**. The upstream (~1500-bp) and downstream (~1000-bp) fragments of

434 HsdMSR open reading frame (ORF) were amplified from the *Psph* genome and
435 digested. Then, the digested upstream and downstream fragments were ligated with
436 T4 DNA ligase (NEB). The ligated fragments were inserted into the digested plasmid
437 using ClonExpress MultiS One Step Cloning Kit (Vazyme). The recombinant
438 plasmids were transformed into the *Psph* WT strain in the KB plate with rifampin and
439 kanamycin. The single colonies were picked to a sucrose plate and then cultured in
440 both KB with kanamycin/rifampin and KB with rifampin alone. Loss of kanamycin
441 resistance indicated a double crossover. Finally, the deletion strains were further
442 confirmed by qRT-PCR to detect the mRNA level of HsdMSR. For the complemented
443 plasmids, the ORF of HsdMS was amplified by PCR from the *Psph* genome and
444 cloned into the pHM1 plasmid.

445 **Growth curve measure assay**

446 Overnight cultures of *Psph* and Δ*hsdMSR* were diluted to an OD600 of 0.1 in fresh
447 KB liquid medium for use as the inoculum. One hundred μL of the inoculum was
448 aliquoted into a 96-well microtiter plate in triplicate and incubated at 28°C for growth.
449 OD600 values were recorded per 2 h for 8 times for plotting of growth curves.

450 **Dot blotting assay**

451 Dot blotting was performed as previously described(70). Briefly, DNA samples were
452 denatured at 95°C for 10 minutes and cooled down on ice for 3 minutes. Samples
453 were spotted on the nylon membrane and air dry for 5 minutes, followed by heat-
454 crosslink at 80 °C for 2 hours. Membranes were blocked in 5% nonfat dry milk in
455 TBST for 1 hour at room temperature, incubated with N6-mA antibodies (1:1000)

456 overnight at 4°C. After 5 washes with TBST, membranes were incubated with HRP-
457 linked secondary anti-rabbit IgG antibody (1:5,000) for 1 hour at room temperature.
458 Signals were detected with ChemiDoc Imaging Systems (Bio-Rad). After imaging,
459 incubate the membrane with methylene blue staining buffer for 15 mins with gentle
460 shaking.

461 **RNA-seq analyses**

462 *Psph* and *ΔhsdMSR* strains were first cultured to the stationary phase in KB at 28°C.
463 Cultures were collected, and total RNA was extracted using a RNeasy mini kit
464 (Qiagen) for subsequent purification with DNaseI (NEB) treatment. After removing
465 rRNA by using the MICROBExpress kit (Ambion), mRNA was used to generate the
466 cDNA library according to the NEBNext® UltraTM II RNA Library Prep Kit protocol
467 (Illumina), which was then sequenced using the Illumina HiSeq 2000 system,
468 generating 150-bp paired-end reads. Two biological replications have been performed.
469 For each RNA-seq sample, raw reads were trimmed using trim_galore (version 0.6.7)
470 and mapped to the *Psph* genome using hisat2 (version 7.5.0)(71). DEGs were
471 identified using DESeq2(72). Function enrichment analysis of DEGs was conducted
472 using the R package clusterProfiler(73).

473 **Ribo-seq library construction and analysis.**

474 The construction of the Ribo-seq library followed the previous protocol(74).
475 Overnight cultures of strains were transferred into fresh KB medium and culture for
476 6 hours, and chloramphenicol was added before centrifugation. The pellet was
477 resuspended in lysis buffer and fast-frozen in liquid nitrogen. MNase then digested

478 the supernatant. Sephacryl S400 MicroSpin columns were used to purify the MNase-
479 digested products. The sRNA was separated using a Zymo RNA kit, and the rRNA
480 was removed. The final library was constructed using the NEBNext Small RNA
481 Library Prep Set. The translational efficiency was calculated by dividing the
482 normalized Ribo-seq counts by the normalized RNA counts.

483 **Real-time quantitative PCR (RT-qPCR) verification**

484 For RT-qPCR, RNA was purified using the RNeasy minikit (Qiagen). The cDNA
485 synthesis was performed using a FastKing RT Kit (Tiangen Biotech). The assay was
486 performed by SuperReal Premix Plus (SYBR Green) Kit (Tiangen Biotech) according
487 to the manufacturer's instruction. Each sample was repeated thrice with 600 ng cDNA
488 and 16S rRNA as the internal control. The fold change represents the relative
489 expression level of mRNA, which can be estimated by the threshold cycle (Ct) values
490 of $2^{-(\Delta\Delta Ct)}$.

491 **Plant infection assay**

492 The bean (*Phaseolus vulgaris* cv. *Red Kidney*) plants were used for the pathogenicity
493 assay. The plant was grown in a greenhouse, as described previously(75). Overnight
494 bacterial cultures were diluted to OD600 = 0.2 × 10−3 and were hand-inoculated into
495 the primary leaves of week-old bean plants for 6 days.

496 **Biofilm formation assay**

497 Biofilm production was detected, as previously reported(76). In brief, overnight
498 bacterial cultures of *Psph* WT and HsdMSR mutants were diluted into OD600 = 0.1
499 and transferred to a 10 ml borosilicate tube containing 1 ml KB medium. Then, the

500 cultures grow statically at 28°C for 3-5 days. Then, 0.1% crystal violet was used to
501 stain the biofilm adhered to the tube tightly for 30 min, and other components bound
502 to the tube loosely were washed off with distilled deionized water. The remaining
503 crystal violet was fully dissolved in 1 ml 95%~100% ethanol with constant shaking.
504 Then, it was transferred to a transparent 96-well plate to measure its optical density at
505 590 nm using a Biotech microplate reader. The experiment was repeated using three
506 independent bacterial cultures.

507 **Data analysis and statistics**

508 The graphs in this paper were plotted using ggplot2 in R 4.2.0 software and GraphPad
509 Prism 10.0.3 (GraphPad Inc.) Differences between groups were analyzed using
510 students' two-tailed t-tests. The results of all statistical analyses are shown as mean ±
511 standard deviation (SD). All experiments were repeated independently at least three
512 times with similar results.

513 **Data availability**

514 The Ribo-seq and RNA-seq data were uploaded to the National Center for
515 Biotechnology Information SRA database as part of BioProject PRJNA1055550.
516 Codes were available upon reasonable request.

517

518 **Acknowledgments**

519 This study was supported by grants from Guangdong Major Project of Basic and
520 Applied Basic Research (2020B0301030005), Shenzhen Science and Technology
521 Fund (JCYJ20210324134000002), the National Natural Science Foundation of China

522 (32172358), General Research Funds of Hong Kong (11103221, 11101722,
523 11102223), the Sichuan Province Science and Technology Planning Project
524 (2021YFSY0005). The funders had no role in study design, data collection,
525 interpretation, or the decision to submit the work for publication.

526

527 **Author contribution**

528 Conceptualization, J.H., and X.D; Methodology, J.H.; Validation, J.H., F.C., B.L., Y.Y.,
529 and Y.S.; Investigation, J.H., F.C. and B.L.; Writing & Editing, J.H., and X.D;
530 Supervision X.D

531

532 **Declare of interest**

533 The authors declare no competing interests.

534

535 **Figure legend**

536 **Figure. 1 Genome-wide identification of *P. syringae* DNA methylation. (A)** The
537 circle map displays the distribution of 6mA, 5mC, and 5mC in *Psph* WT. **(B)** The
538 Venn plot reveals overlapped genes within three types of DNA methylation of *Psph*
539 WT. **(C)** The circle map displays the distribution of 6mA, 5mC, and 5mC in *Pst* WT.
540 **(D)** The Venn plot reveals overlapped genes within three types of DNA methylation of
541 *Pst* WT. **(E)** The circle map displays the distribution of 6mA, 5mC, and 5mC in *Pss*
542 WT. **(F)** The Venn plot reveals overlapped genes within three types of DNA
543 methylation of *Pss* WT.

544 **Figure. 2 Functional enrichment analysis of methylation sites in three *P. syringae***
545 **strains. (A)** Repartition of the total pool of modified genes among strains. **(B)**
546 Proportion of methylated genes detected in one, two, or three genomes for all *P.*
547 *syringae* strains and conserved DNA methylation sites with detected genes. **(C)** The
548 dot plot reveals the functional annotation enrichment of genes within different
549 modified bases among three strains in GO and KEGG terms. The size of the dots
550 indicates the number of related genes.

551 **Figure. 3 DNA methylation motifs in *P. syringae*. (A)** 6mA methylation motifs
552 found in *Psph* using SMRT-seq. The black arrows indicate the site of adenine
553 methylation. **(B)** Bar plot shows the abundance of methylated numbers throughout all
554 motif sites in *Psph*. **(C)** 6mA and 4mC methylation motifs found in *Pst* using SMRT-
555 seq. The black arrows indicate the site of base methylation. **(D)** Bar plot shows the
556 abundance of methylated numbers throughout all motif sites in *Pst*.

557 **Figure. 4 Transcriptional changes profiling of *hsdMSR* mutant in *Psph*. (A)** The
558 volcano plot reveals DEGs between *Psph* WT and Δ*hsdMSR*. The DEGs were ($|\log_2$
559 $FC| > 1$ and adjusted P value < 0.05) in blue (Ribosomal protein), pink (Alginate
560 biosynthesis), and yellow (T3SS). Each dot represents one gene. **(B)** Bubble plot
561 shows enriched GO (Red) and KEGG (Blue) terms based on the DEGs between *Psph*
562 WT and Δ*hsdMSR*. The x-axis shows the significance of functional annotation terms
563 (−log10 adjusted *P*-value), and the y-axis indicates the Z-score of terms. The bubble
564 size represents the gene number of terms. **(C)** COG classification and distribution of
565 up-regulated DEGs. **(D)** COG classification and distribution of down-regulated DEGs.

566 COG terms are highlighted in different colors. **(E)** Venn plot reveals the overlapped
567 genes between DEGs and genes within the HsdMSR motif.

568 **Figure. 5 Influence of HsdMSR on virulence and metabolism in *Psph*. (A)**
569 HsdMSR negatively regulated T3SS-related genes. Data are shown as means ± SD (n
570 = 3). **(B)** Disease symptoms caused by *Psph* WT, Δ*hsdMSR*, and the complemented
571 strains, photographing 6 days after inoculation of 10^5 CFU/mL bacteria. **(C)** HsdMSR
572 negatively regulated alginate biosynthesis-related genes. Data are shown as means ±
573 SD (n = 3). **(D)** The quantification of biofilm production in the *Psph* WT, Δ*hsdMSR*,
574 and the complemented strains using a crystal violate staining assay. **(E)** HsdMSR
575 positively regulated ribosomal protein-related genes. Data are shown as means ± SD
576 (n = 3). **(F)** The scatterplot shows the TE and mRNA change between *Psph* WT and
577 Δ*hsdMSR*. The x-axis presents the log2FC of the mRNA level, and the y-axis shows
578 the $\log_2$FC of the TE. The greater TE is represented in red, whereas the lesser TE is
579 displayed in blue.

580 **Figure. 6 6mA methylation regulates gene transcription based on fully**
581 **methylated. (A)** Upstream region sequence of *hrpF* carrying the HsdMSR motif.
582 Adenine methylation is highlighted in red. **(B)** Constantly lux activity detection of the
583 *hrpF* between *Psph* WT and Δ*hsdMSR*. **(C)** Lux activity of *hrpF* between *Psph* WT
584 and Δ*hsdMSR* at the time point 24 hours. **(D)** Lux activity of *hrpF* between *Psph* WT
585 and Δ*hsdMSR* with point mutation. In the HsdMSR motif, an "A" was replaced by a
586 "C", highlighted in bold and underlined. **(E)** Lux activity of *hrpF* between *Psph* WT
587 and Δ*hsdMSR* with double point mutations. In the HsdMSR motif, two "A" was

588 replaced by a “C”, highlighted in bold and underlined.

589 **Figure. S1 Distribution patterns of methylation sites in three model strains. (A)**
590 Bar plot shows the distribution of modified sites located in different regions of CDS,
591 intergenic region, and non-coding RNA. **(B)** GC contents distribution of 6mA
592 between three *P. syringae* strains. **(C)** GC contents distribution of 5mC between three
593 *P. syringae* strains. **(D)** GC contents distribution of 4mC between three *P. syringae*
594 strains.

595 **Figure. S2 COG analysis of methylation sites in *P. syringae*. (A)** COG
596 classification of three DNA methylations in *Psph*. **(B)** COG classification of three
597 DNA methylations in *Pst*. **(C)** COG classification of three DNA methylations in *Pss*.

598 **Figure. S3 Comparative genomic analysis of Type I RM system among bacterial**
599 **species.** Different species are highlighted in different colors. The color key indicates
600 the %identity compared to the MTases in *Psph*.

601 **Figure. S4 Growth curve of *Psph* WT, Δ*hsdMSR*, and complemented strains at**
602 **28°C in KB medium.**

603 **Figure. S5 Identification of Type I DNA methyltransferase in *Psph*. (A)** Dot blot
604 reveals stationary phase of *Psph* has higher 6mA methylation level. **(B)** HsdMSR can
605 catalyze 6mA formation in *Psph*. **(C)** SMRT-seq reveals HsdMSR catalyzed the 6mA
606 motif C**A**GCN$_{(6)}$CTC.

607 **Figure. S6 Number of genes with significant TE changes. (A)** The GO terms for the
608 genes in which TE changed more than 1-FC. **(B)** The GO terms for the genes in which
609 TE changed less than 1-FC.

610 **Table S1 Restriction-modification systems predicted in *P. syringae*.**

611 **Table S2 Modified genes conserved in three *P. syringae* strains.**

612 **Table S3 DEGs genes between *Psph* WT and Δ*hsdMSR*.**

613 **Table S4 DEGs carrying HsdMSR motif in their putative promoter regions.**

614 **Table S5 Genes with changed TE between *Psph* WT and Δ*hsdMSR*.**

615 **Table S6 Strains, plasmids, and primers.**

616

617

618 **References**

619

620 1. Bull CT, De Boer SH, Denny TP, Firrao G, Saux MF-L, Saddler GS,
621 Scortichini M, Stead DE, Takikawa Y. 2010. Comprehensive list of names of
622 plant pathogenic bacteria, 1980-2007. Journal of Plant Pathology:551-592.
623 2. Xin X-F, Kvitko B, He SY. 2018. *Pseudomonas syringae*: what it takes to be a
624 pathogen. Nature Reviews Microbiology 16:316-328.
625 3. Arnold DL, Lovell HC, Jackson RW, Mansfield JW. 2011. *Pseudomonas*
626 *syringae* pv. *phaseolicola*: from 'has bean' to supermodel. Molecular Plant
627 Pathology 12:617-627.
628 4. Xin XF, He SY. 2013. *Pseudomonas syringae* pv. *tomato* DC3000: a model
629 pathogen for probing disease susceptibility and hormone signaling in plants.
630 Annu Rev Phytopathol 51:473-98.
631 5. Monier JM, Lindow SE. 2005. Aggregates of resident bacteria facilitate
632 survival of immigrant bacteria on leaf surfaces. Microb Ecol 49:343-52.
633 6. Clarke CR, Cai R, Studholme DJ, Guttman DS, Vinatzer BA. 2010.
634 *Pseudomonas syringae* strains naturally lacking the classical *P. syringae*
635 hrp/hrc Locus are common leaf colonizers equipped with an atypical type III
636 secretion system. Mol Plant Microbe Interact 23:198-210.
637 7. Rahme LG, Mindrinos MN, Panopoulos NJ. 1992. Plant and environmental
638 sensory signals control the expression of hrp genes in *Pseudomonas syringae*
639 pv. *phaseolicola*. J Bacteriol 174:3499-507.
640 8. Xiao F, Goodwin SM, Xiao Y, Sun Z, Baker D, Tang X, Jenks MA, Zhou JM.
641 2004. *Arabidopsis* CYP86A2 represses *Pseudomonas syringae* type III genes
642 and is required for cuticle development. EMBO J 23:2903-13.
643 9. Xiao Y, Lu Y, Heu S, Hutcheson SW. 1992. Organization and environmental
644 regulation of the *Pseudomonas syringae* pv. *syringae* 61 hrp cluster. J
645 Bacteriol 174:1734-41.
646 10. Xiao Y, Heu S, Yi J, Lu Y, Hutcheson SW. 1994. Identification of a putative
647 alternate sigma factor and characterization of a multicomponent regulatory
648 cascade controlling the expression of *Pseudomonas syringae* pv. *syringae*
649 Pss61 *hrp* and *hrmA* genes. J Bacteriol 176:1025-36.
650 11. Hutcheson SW, Bretz J, Sussan T, Jin S, Pak K. 2001. Enhancer-binding
651 proteins HrpR and HrpS interact to regulate hrp-encoded type III protein
652 secretion in *Pseudomonas syringae* strains. J Bacteriol 183:5589-98.
653 12. Hendrickson EL, Guevera P, Ausubel FM. 2000. The alternative sigma factor
654 RpoN is required for hrp activity in *Pseudomonas syringae* pv. *maculicola* and
655 acts at the level of *hrpL* transcription. Journal of bacteriology 182:3508-3516.
656 13. Haefele DM, Lindow SE. 1987. Flagellar motility confers epiphytic fitness
657 advantages upon *Pseudomonas syringae*. Applied and Environmental
658 Microbiology 53:2528-2533.
659 14. Dasgupta N, Wolfgang MC, Goodman AL, Arora SK, Jyot J, Lory S, Ramphal

660 R. 2003. A four-tiered transcriptional regulatory circuit controls flagellar
661 biogenesis in *Pseudomonas aeruginosa* pv. *tomato* DC3000. Mol Microbiol
662 50:809-24.
663 15. Deng X, Liang H, Chen K, He C, Lan L, Tang X. 2014. Molecular
664 mechanisms of two-component system RhpRS regulating type III secretion
665 system in *Pseudomonas syringae*. Nucleic Acids Res 42:11472-86.
666 16. Fan L, Wang T, Hua C, Sun W, Li X, Grunwald L, Liu J, Wu N, Shao X, Yin Y,
667 Yan J, Deng X. 2020. A compendium of DNA-binding specificities of
668 transcription factors in *Pseudomonas syringae*. Nat Commun 11:4947.
669 17. Xie Y, Ding Y, Shao X, Yao C, Li J, Liu J, Deng X. 2021. *Pseudomonas*
670 *syringae* senses polyphenols via phosphorelay crosstalk to inhibit virulence.
671 EMBO Rep 22:e52805.
672 18. Shao X, Tan M, Xie Y, Yao C, Wang T, Huang H, Zhang Y, Ding Y, Liu J, Han
673 L, Hua C, Wang X, Deng X. 2021. Integrated regulatory network in
674 *Pseudomonas syringae* reveals dynamics of virulence. Cell Rep 34:108920.
675 19. Huang J, Yao C, Sun Y, Ji Q, Deng X. 2022. Virulence-related regulatory
676 network of *Pseudomonas syringae*. Comput Struct Biotechnol J 20:6259-6270.
677 20. Gold M, Hurwitz J, Anders M. 1963. The enzymatic methylation of RNA and
678 DNA, II. On the species specificity of the methylation enzymes. Proceedings
679 of the National Academy of Sciences 50:164-169.
680 21. Casadesus J, Low D. 2006. Epigenetic gene regulation in the bacterial world.
681 Microbiol Mol Biol Rev 70:830-56.
682 22. Wion D, Casadesus J. 2006. N6-methyl-adenine: an epigenetic signal for
683 DNA-protein interactions. Nat Rev Microbiol 4:183-92.
684 23. Bickle TA, Kruger DH. 1993. Biology of DNA restriction. Microbiol Rev
685 57:434-50.
686 24. Loenen WA, Dryden DT, Raleigh EA, Wilson GG. 2014. Type I restriction
687 enzymes and their relatives. Nucleic Acids Res 42:20-44.
688 25. Blow MJ, Clark TA, Daum CG, Deutschbauer AM, Fomenkov A, Fries R,
689 Froula J, Kang DD, Malmstrom RR, Morgan RD, Posfai J, Singh K, Visel A,
690 Wetmore K, Zhao Z, Rubin EM, Korlach J, Pennacchio LA, Roberts RJ. 2016.
691 The Epigenomic Landscape of Prokaryotes. PLoS Genet 12:e1005854.
692 26. Beaulaurier J, Schadt EE, Fang G. 2019. Deciphering bacterial epigenomes
693 using modern sequencing technologies. Nat Rev Genet 20:157-172.
694 27. Ho J, Taiaroa G, Butler MI, Poulter RTM. 2019. The Genome Sequence of
695 M228, a Chinese Isolate of *Pseudomonas syringae* pv. actinidiae, Illustrates
696 Insertion Sequence Element Mobility. Microbiol Resour Announc 8.
697 28. Poulter RTM, Ho J, Handley T, Taiaroa G, Butler MI. 2018. Comparison
698 between complete genomes of an isolate of *Pseudomonas syringae* pv.
699 actinidiae from Japan and a New Zealand isolate of the pandemic lineage.
700 Scientific Reports 8.
701 29. Poulter R, Taiaroa G, Sumpter N, Stockwell P, Butler M. 2017. Complete
702 Genome Sequence of the Kiwifruit Pathogen *Pseudomonas syringae* pv.
703 actinidiae Biovar 5, Originating from Japan. Genome Announc 5.

30. Doberenz S, Eckweiler D, Reichert O, Jensen V, Bunk B, Sproer C, Kordes A, Frangipani E, Luong K, Korlach J, Heeb S, Overmann J, Kaever V, Haussler S. 2017. Identification of a *Pseudomonas aeruginosa* PAO1 DNA Methyltransferase, Its Targets, and Physiological Roles. mBio 8.
31. Han S, Liu J, Li M, Zhang Y, Duan X, Zhang Y, Chen H, Cai Z, Yang L, Liu Y. 2022. DNA Methyltransferase Regulates Nitric Oxide Homeostasis and Virulence in a Chronically Adapted *Pseudomonas aeruginosa* Strain. mSystems 7:e0043422.
32. Li Z, Zhou X, Liao D, Liu R, Zhao X, Wang J, Zhong Q, Zeng Z, Peng Y, Tan Y, Yang Z. 2023. Comparative genomics and DNA methylation analysis of *Pseudomonas aeruginosa* clinical isolate PA3 by single-molecule real-time sequencing reveals new targets for antimicrobials. Front Cell Infect Microbiol 13:1180194.
33. Roberts RJ, Vincze T, Posfai J, Macelis D. 2023. REBASE: a database for DNA restriction and modification: enzymes, genes and genomes. Nucleic Acids Res 51:D629-D630.
34. Bird A. 2002. DNA methylation patterns and epigenetic memory. Genes & development 16:6-21.
35. Gelfman S, Cohen N, Yearim A, Ast G. 2013. DNA-methylation effect on cotranscriptional splicing is dependent on GC architecture of the exon–intron structure. Genome research 23:789-799.
36. Militello KT, Simon RD, Qureshi M, Maines R, Van Horne ML, Hennick SM, Jayakar SK, Pounder S. 2012. Conservation of Dcm-mediated cytosine DNA methylation in *Escherichia coli*. FEMS microbiology letters 328:78-85.
37. Nur I, Szyf M, Razin A, Glaser G, Rottem S, Razin S. 1985. Procaryotic and eucaryotic traits of DNA methylation in spiroplasmas (mycoplasmas). Journal of bacteriology 164:19-24.
38. Ashburner M, Ball CA, Blake JA, Botstein D, Butler H, Cherry JM, Davis AP, Dolinski K, Dwight SS, Eppig JT, Harris MA, Hill DP, Issel-Tarver L, Kasarskis A, Lewis S, Matese JC, Richardson JE, Ringwald M, Rubin GM, Sherlock G. 2000. Gene ontology: tool for the unification of biology. The Gene Ontology Consortium. Nat Genet 25:25-9.
39. Kanehisa M, Goto S. 2000. KEGG: kyoto encyclopedia of genes and genomes. Nucleic Acids Res 28:27-30.
40. Cantalapiedra CP, Hernandez-Plaza A, Letunic I, Bork P, Huerta-Cepas J. 2021. eggNOG-mapper v2: Functional Annotation, Orthology Assignments, and Domain Prediction at the Metagenomic Scale. Mol Biol Evol 38:5825-5829.
41. Huerta-Cepas J, Szklarczyk D, Heller D, Hernandez-Plaza A, Forslund SK, Cook H, Mende DR, Letunic I, Rattei T, Jensen LJ, von Mering C, Bork P. 2019. eggNOG 5.0: a hierarchical, functionally and phylogenetically annotated orthology resource based on 5090 organisms and 2502 viruses. Nucleic Acids Res 47:D309-D314.
42. Bailey TL, Johnson J, Grant CE, Noble WS. 2015. The MEME Suite. Nucleic

748 Acids Res 43:W39-49.
749 43. Boyd A, Chakrabarty A. 1995. *Pseudomonas aeruginosa* biofilms: role of the
750 alginate exopolysaccharide. Journal of industrial microbiology and
751 biotechnology 15:162-168.
752 44. Ichinose Y, Taguchi F, Mukaihara T. 2013. Pathogenicity and virulence factors
753 of *Pseudomonas syringae*. Journal of General Plant Pathology 79:285-296.
754 45. Zhou X, Liao WJ, Liao JM, Liao P, Lu H. 2015. Ribosomal proteins: functions
755 beyond the ribosome. J Mol Cell Biol 7:92-104.
756 46. Murray IA, Clark TA, Morgan RD, Boitano M, Anton BP, Luong K,
757 Fomenkov A, Turner SW, Korlach J, Roberts RJ. 2012. The methylomes of six
758 bacteria. Nucleic Acids Res 40:11450-62.
759 47. Lee WC, Anton BP, Wang S, Baybayan P, Singh S, Ashby M, Chua EG, Tay
760 CY, Thirriot F, Loke MF, Goh KL, Marshall BJ, Roberts RJ, Vadivelu J. 2015.
761 The complete methylome of *Helicobacter pylori* UM032. BMC Genomics
762 16:424.
763 48. Fang CT, Yi WC, Shun CT, Tsai SF. 2017. DNA adenine methylation
764 modulates pathogenicity of Klebsiella pneumoniae genotype K1. J Microbiol
765 Immunol Infect 50:471-477.
766 49. Kumar S, Karmakar BC, Nagarajan D, Mukhopadhyay AK, Morgan RD, Rao
767 DN. 2018. N4-cytosine DNA methylation regulates transcription and
768 pathogenesis in *Helicobacter pylori*. Nucleic Acids Res 46:3815.
769 50. Seong HJ, Park HJ, Hong E, Lee SC, Sul WJ, Han SW. 2016. Methylome
770 Analysis of Two *Xanthomonas* spp. Using Single-Molecule Real-Time
771 Sequencing. Plant Pathol J 32:500-507.
772 51. Park HJ, Jung B, Lee J, Han SW. 2019. Functional characterization of a
773 putative DNA methyltransferase, EadM, in *Xanthomonas axonopodis* pv.
774 *glycines* by proteomic and phenotypic analyses. Sci Rep 9:2446.
775 52. Park HJ, Seong HJ, Lee J, Heo L, Sul WJ, Han SW. 2021. Two DNA
776 Methyltransferases for Site-Specific 6mA and 5mC DNA Modification in
777 *Xanthomonas euvesicatoria*. Front Plant Sci 12:621466.
778 53. Krebes J, Morgan RD, Bunk B, Spröer C, Luong K, Parusel R, Anton BP,
779 König C, Josenhans C, Overmann J. 2014. The complex methylome of the
780 human gastric pathogen *Helicobacter pylori*. Nucleic acids research 42:2415-
781 2432.
782 54. Bourgeois JS, Anderson CE, Wang L, Modliszewski JL, Chen W, Schott BH,
783 Devos N, Ko DC. 2022. Integration of the *Salmonella Typhimurium*
784 Methylome and Transcriptome Reveals That DNA Methylation and
785 Transcriptional Regulation Are Largely Decoupled under Virulence-Related
786 Conditions. mBio 13:e0346421.
787 55. Reyes-Lamothe R, Sherratt DJ. 2019. The bacterial cell cycle, chromosome
788 inheritance and cell growth. Nat Rev Microbiol 17:467-478.
789 56. Gonzalez D, Kozdon JB, McAdams HH, Shapiro L, Collier J. 2014. The
790 functions of DNA methylation by CcrM in *Caulobacter crescentus*: a global
791 approach. Nucleic Acids Res 42:3720-35.

792 57. Kozdon JB, Melfi MD, Luong K, Clark TA, Boitano M, Wang S, Zhou B,
793 Gonzalez D, Collier J, Turner SW, Korlach J, Shapiro L, McAdams HH. 2013.
794 Global methylation state at base-pair resolution of the *Caulobacter* genome
795 throughout the cell cycle. Proceedings of the National Academy of Sciences
796 110:E4658-E4667.
797 58. Seong HJ, Han SW, Sul WJ. 2021. Prokaryotic DNA methylation and its
798 functional roles. J Microbiol 59:242-248.
799 59. Boye E, Stokke T, Kleckner N, Skarstad K. 1996. Coordinating DNA
800 replication initiation with cell growth: differential roles for DnaA and SeqA
801 proteins. Proc Natl Acad Sci U S A 93:12206-11.
802 60. Manzer HS, Brunetti T, Doran KS. Identification of a DNA-cytosine
803 methyltransferase that impacts global transcription to promote group B
804 streptococcal vaginal colonization. mBio 0:e02306-23.
805 61. Banas JA, Biswas S, Zhu M. 2011. Effects of DNA methylation on expression
806 of virulence genes in *Streptococcus* mutans. Appl Environ Microbiol 77:7236-
807 42.
808 62. Oliveira PH, Ribis JW, Garrett EM, Trzilova D, Kim A, Sekulovic O, Mead
809 EA, Pak T, Zhu S, Deikus G. 2020. Epigenomic characterization of
810 *Clostridioides difficile* finds a conserved DNA methyltransferase that mediates
811 sporulation and pathogenesis. Nature microbiology 5:166-180.
812 63. Lim HN, van Oudenaarden A. 2007. A multistep epigenetic switch enables the
813 stable inheritance of DNA methylation states. Nat Genet 39:269-75.
814 64. Kahramanoglou C, Prieto AI, Khedkar S, Haase B, Gupta A, Benes V, Fraser
815 GM, Luscombe NM, Seshasayee AS. 2012. Genomics of DNA cytosine
816 methylation in *Escherichia coli* reveals its role in stationary phase
817 transcription. Nat Commun 3:886.
818 65. Rishi V, Bhattacharya P, Chatterjee R, Rozenberg J, Zhao J, Glass K,
819 Fitzgerald P, Vinson C. 2010. CpG methylation of half-CRE sequences creates
820 C/EBPα binding sites that activate some tissue-specific genes. Proceedings of
821 the National Academy of Sciences 107:20311-20316.
822 66. Diekmann S. 1987. DNA methylation can enhance or induce DNA curvature.
823 The EMBO journal 6:4213-4217.
824 67. Camacho EM, Serna A, Madrid C, Marques S, Fernandez R, de la Cruz F,
825 Juarez A, Casadesus J. 2005. Regulation of finP transcription by DNA adenine
826 methylation in the virulence plasmid of *Salmonella enterica*. J Bacteriol
827 187:5691-9.
828 68. Xie Y, Li J, Ding Y, Shao X, Sun Y, Xie F, Liu S, Tang S, Deng X. 2022. An
829 atlas of bacterial two-component systems reveals function and plasticity in
830 signal transduction. Cell Rep 41:111502.
831 69. Kvitko BH, Collmer A. 2011. Construction of *Pseudomonas syringae* pv.
832 *tomato* DC3000 mutant and polymutant strains. Methods Mol Biol 712:109-28.
833 70. Xie Q, Wu TP, Gimple RC, Li Z, Prager BC, Wu Q, Yu Y, Wang P, Wang Y,
834 Gorkin DU. 2018. N6-methyladenine DNA modification in glioblastoma. Cell
835 175:1228-1243. e20.

836 71. Kim D, Langmead B, Salzberg SL. 2015. HISAT: a fast spliced aligner with
837 low memory requirements. Nat Methods 12:357-60.
838 72. Love MI, Huber W, Anders S. 2014. Moderated estimation of fold change and
839 dispersion for RNA-seq data with DESeq2. Genome biology 15:1-21.
840 73. Yu G, Wang L-G, Han Y, He Q-Y. 2012. clusterProfiler: an R package for
841 comparing biological themes among gene clusters. Omics: a journal of
842 integrative biology 16:284-287.
843 74. Hua C, Huang J, Wang T, Sun Y, Liu J, Huang L, Deng X. 2022. Bacterial
844 Transcription Factors Bind to Coding Regions and Regulate Internal Cryptic
845 Promoters. mBio 13:e0164322.
846 75. Xiao Y, Lan L, Yin C, Deng X, Baker D, Zhou JM, Tang X. 2007. Two-
847 component sensor RhpS promotes induction of *Pseudomonas syringae* type III
848 secretion system by repressing negative regulator RhpR. Mol Plant Microbe
849 Interact 20:223-34.
850 76. Shao X, Xie Y, Zhang Y, Deng X. 2019. Biofilm Formation Assay in
851 *Pseudomonas syringae*. Bio Protoc 9:e3237.

852

Figure 1

A

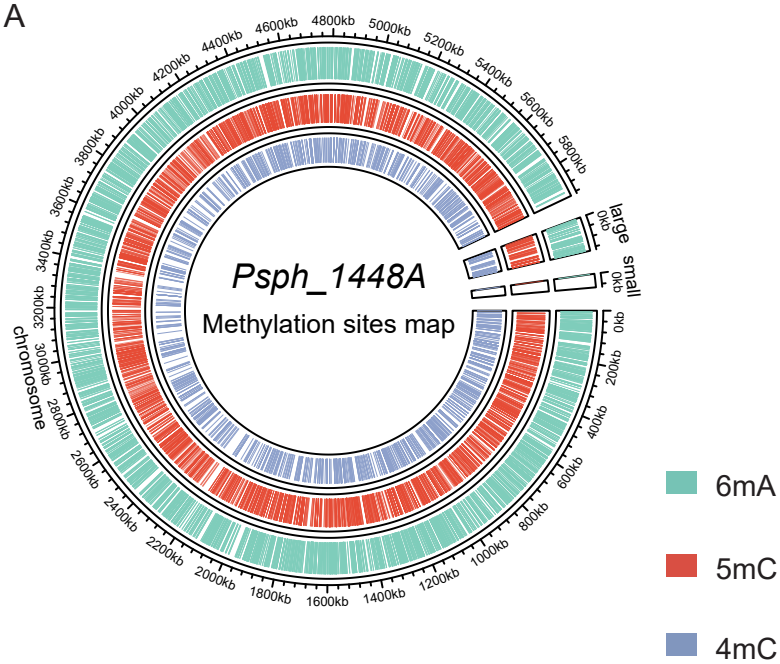

B

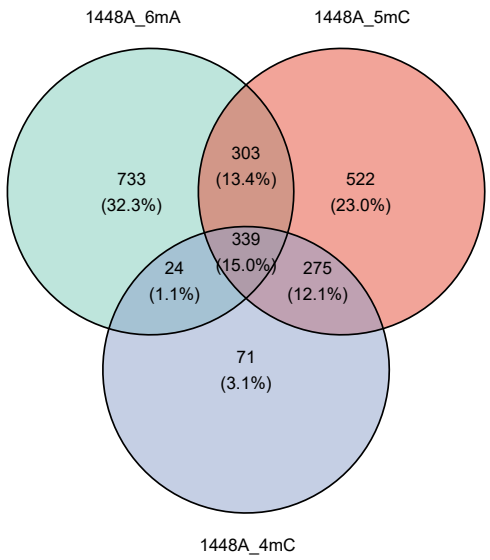

C

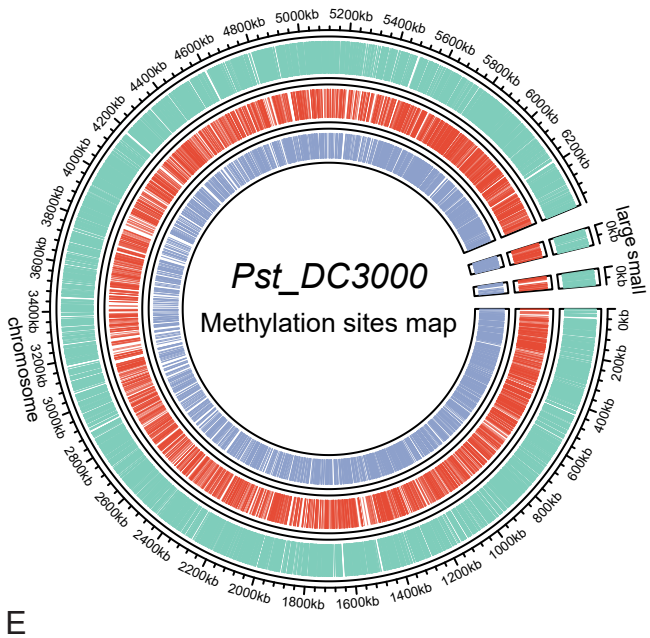

D

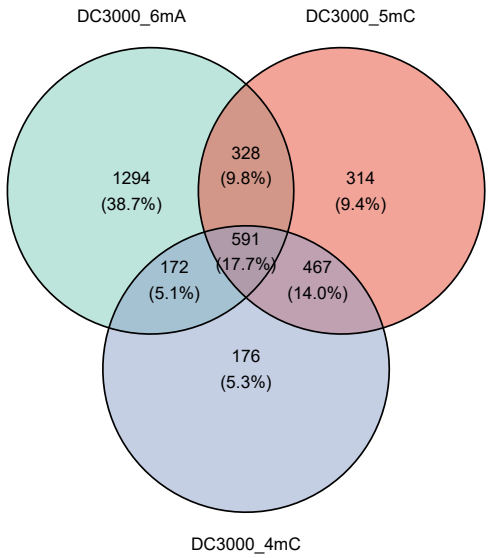

E

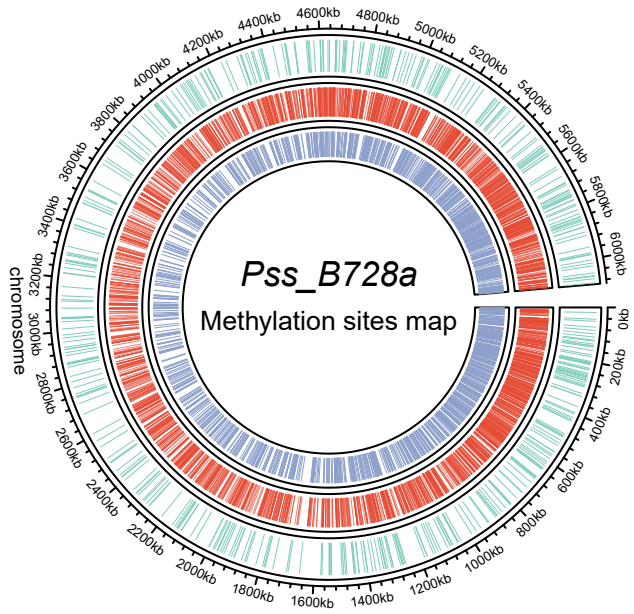

F

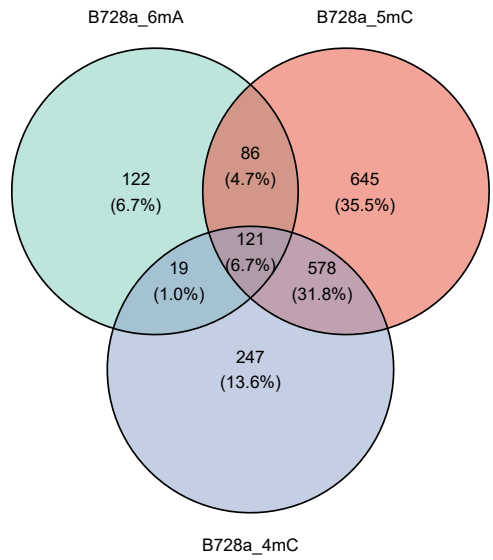

Figure 2

A

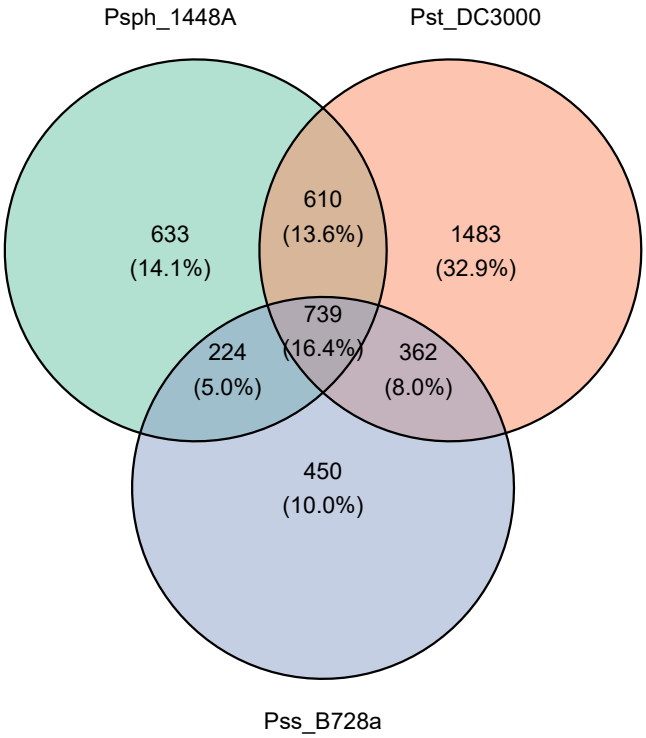
Psph_1448A
Pst_DC3000
Pss_B728a
633
(14.1%)
610
(13.6%)
1483
(32.9%)
739
(16.4%)
224
(5.0%)
362
(8.0%)
450
(10.0%)

B

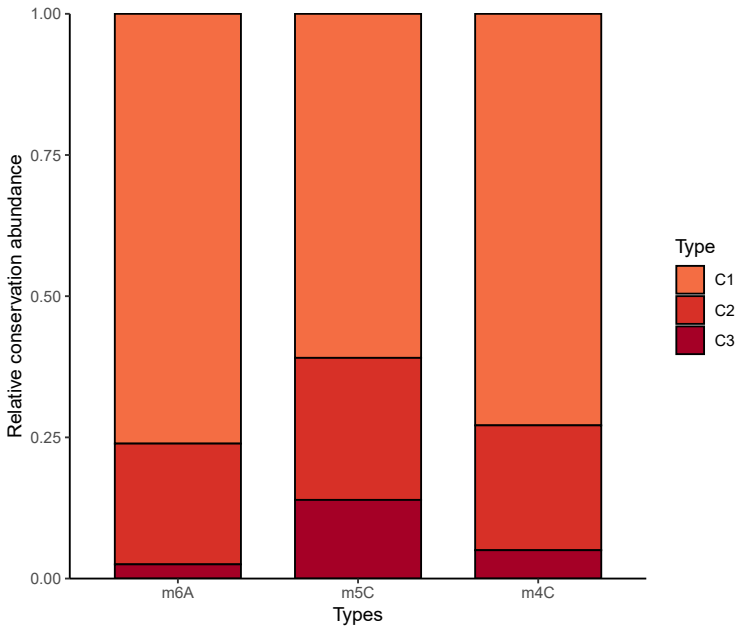
Relative conservation abundance
1.00
0.75
0.50
0.25
0.00
m6A
m5C
m4C
Types
Type
C1
C2
C3

C

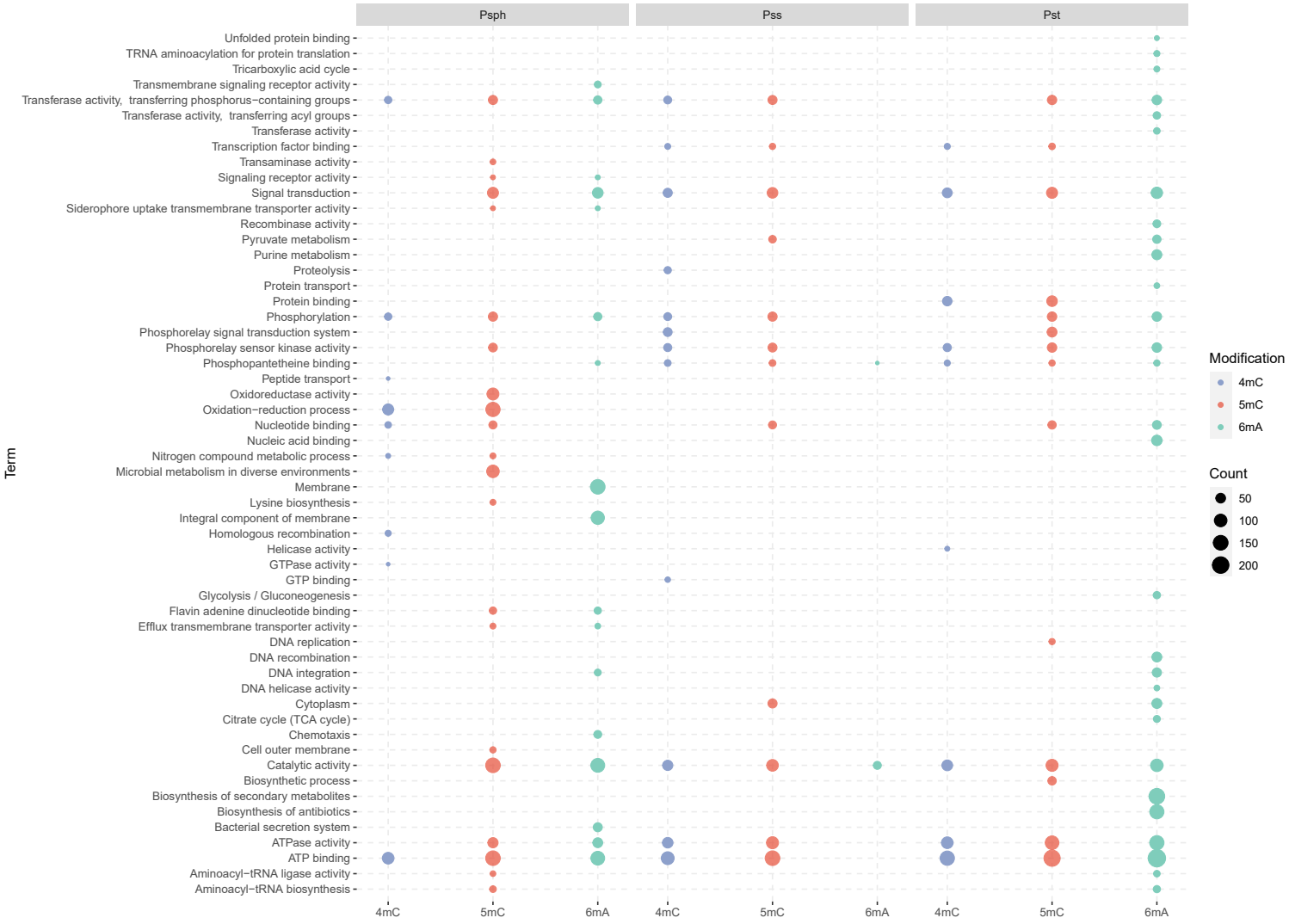
Psph
Pss
Pst
Term
Unfolded protein binding
TRNA aminoacylation for protein translation
Tricarboxylic acid cycle
Transmembrane signaling receptor activity
Transferase activity, transferring phosphorus−containing groups
Transferase activity, transferring acyl groups
Transferase activity
Transcription factor binding
Transaminase activity
Signaling receptor activity
Signal transduction
Siderophore uptake transmembrane transporter activity
Recombinase activity
Pyruvate metabolism
Purine metabolism
Proteolysis
Protein transport
Protein binding
Phosphorylation
Phosphorelay signal transduction system
Phosphorelay sensor kinase activity
Phosphopantetheine binding
Peptide transport
Oxidoreductase activity
Oxidation−reduction process
Nucleotide binding
Nucleic acid binding
Nitrogen compound metabolic process
Microbial metabolism in diverse environments
Membrane
Lysine biosynthesis
Integral component of membrane
Homologous recombination
Helicase activity
GTPase activity
GTP binding
Glycolysis / Gluconeogenesis
Flavin adenine dinucleotide binding
Efflux transmembrane transporter activity
DNA replication
DNA recombination
DNA integration
DNA helicase activity
Cytoplasm
Citrate cycle (TCA cycle)
Chemotaxis
Cell outer membrane
Catalytic activity
Biosynthetic process
Biosynthesis of secondary metabolites
Biosynthesis of antibiotics
Bacterial secretion system
ATPase activity
ATP binding
Aminoacyl−tRNA ligase activity
Aminoacyl−tRNA biosynthesis
4mC
5mC
6mA
Modification
4mC
5mC
6mA
Count
50
100
150
200

Figure 3

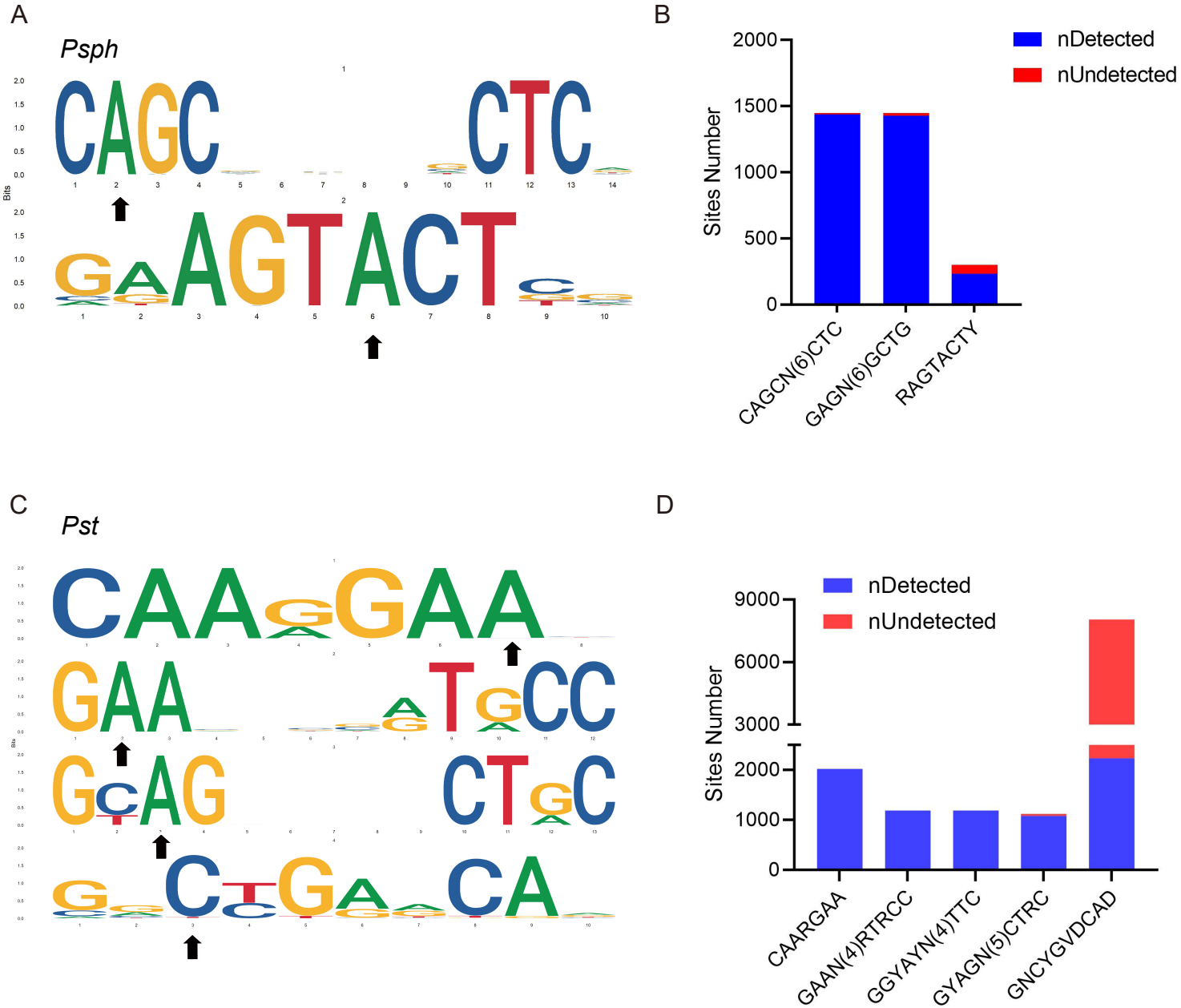
A
Psph
Bits
B
nDetected
nUndetected
Sites Number
2000
1500
1000
500
0
CAGCN(6)CTC
GAGN(6)GCTG
RAGTACTY
C
Pst
D
nDetected
nUndetected
Sites Number
9000
6000
3000
2000
1000
0
CAARGAA
GAAN(4)RTRCC
GGYAYN(4)TTC
GYAGN(5)CTRC
GNCYGVDCAD

Figure 4

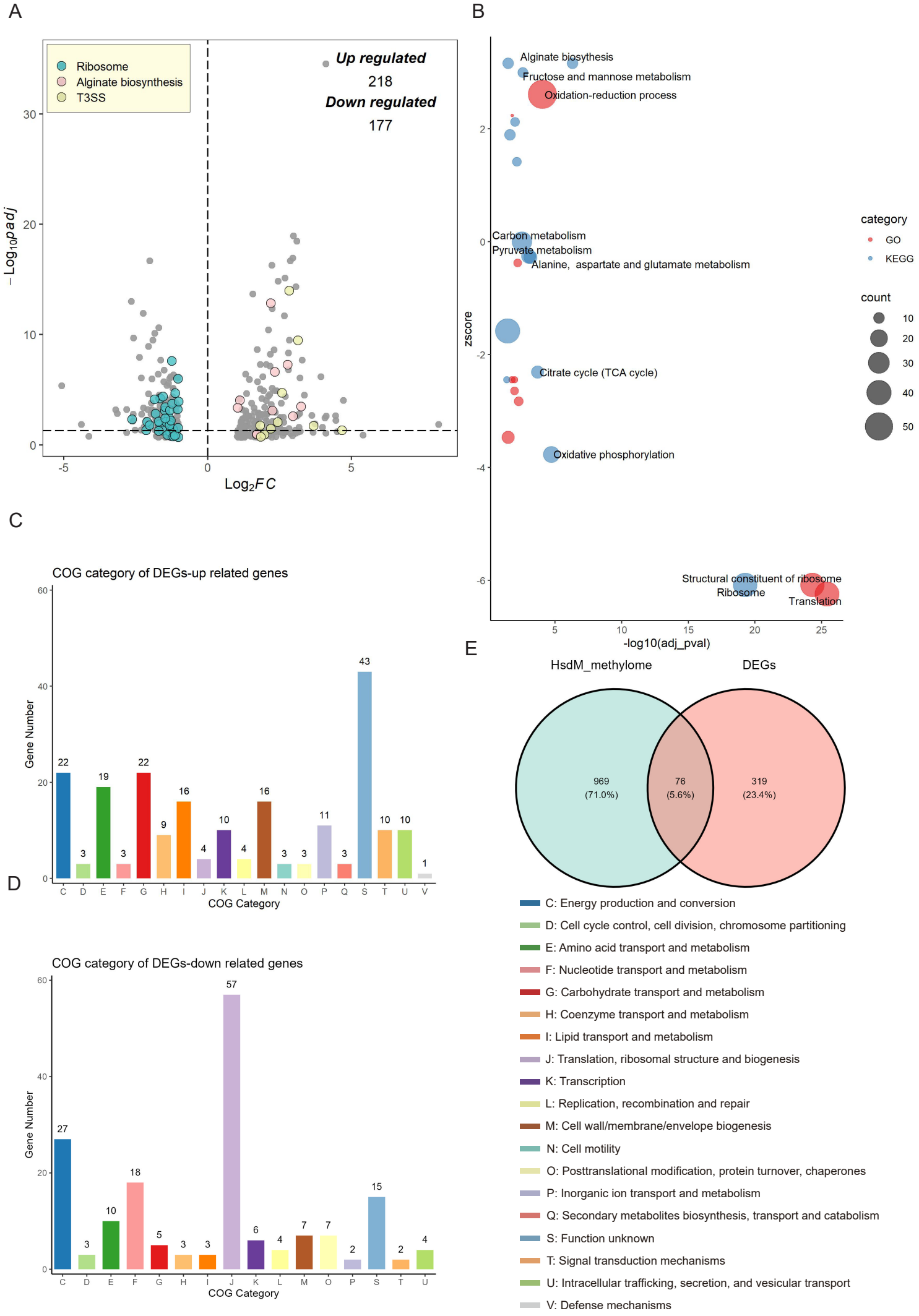
A
Ribosome
Alginate biosynthesis
T3SS
Up regulated
218
Down regulated
177
$-Log_{10}padj$
Log_2FC
B
Alginate biosythesis
Fructose and mannose metabolism
Oxidation-reduction process
Carbon metabolism
Pyruvate metabolism
Alanine, aspartate and glutamate metabolism
Citrate cycle (TCA cycle)
Oxidative phosphorylation
Structural constituent of ribosome
Ribosome
Translation
zscore
-log10(adj_pval)
category
GO
KEGG
count
C
COG category of DEGs-up related genes
Gene Number
COG Category
D
COG category of DEGs-down related genes
E
HsdM_methylome
DEGs
969
(71.0%)
76
(5.6%)
319
(23.4%)
C: Energy production and conversion
D: Cell cycle control, cell division, chromosome partitioning
E: Amino acid transport and metabolism
F: Nucleotide transport and metabolism
G: Carbohydrate transport and metabolism
H: Coenzyme transport and metabolism
I: Lipid transport and metabolism
J: Translation, ribosomal structure and biogenesis
K: Transcription
L: Replication, recombination and repair
M: Cell wall/membrane/envelope biogenesis
N: Cell motility
O: Posttranslational modification, protein turnover, chaperones
P: Inorganic ion transport and metabolism
Q: Secondary metabolites biosynthesis, transport and catabolism
S: Function unknown
T: Signal transduction mechanisms
U: Intracellular trafficking, secretion, and vesicular transport
V: Defense mechanisms

Figure 5

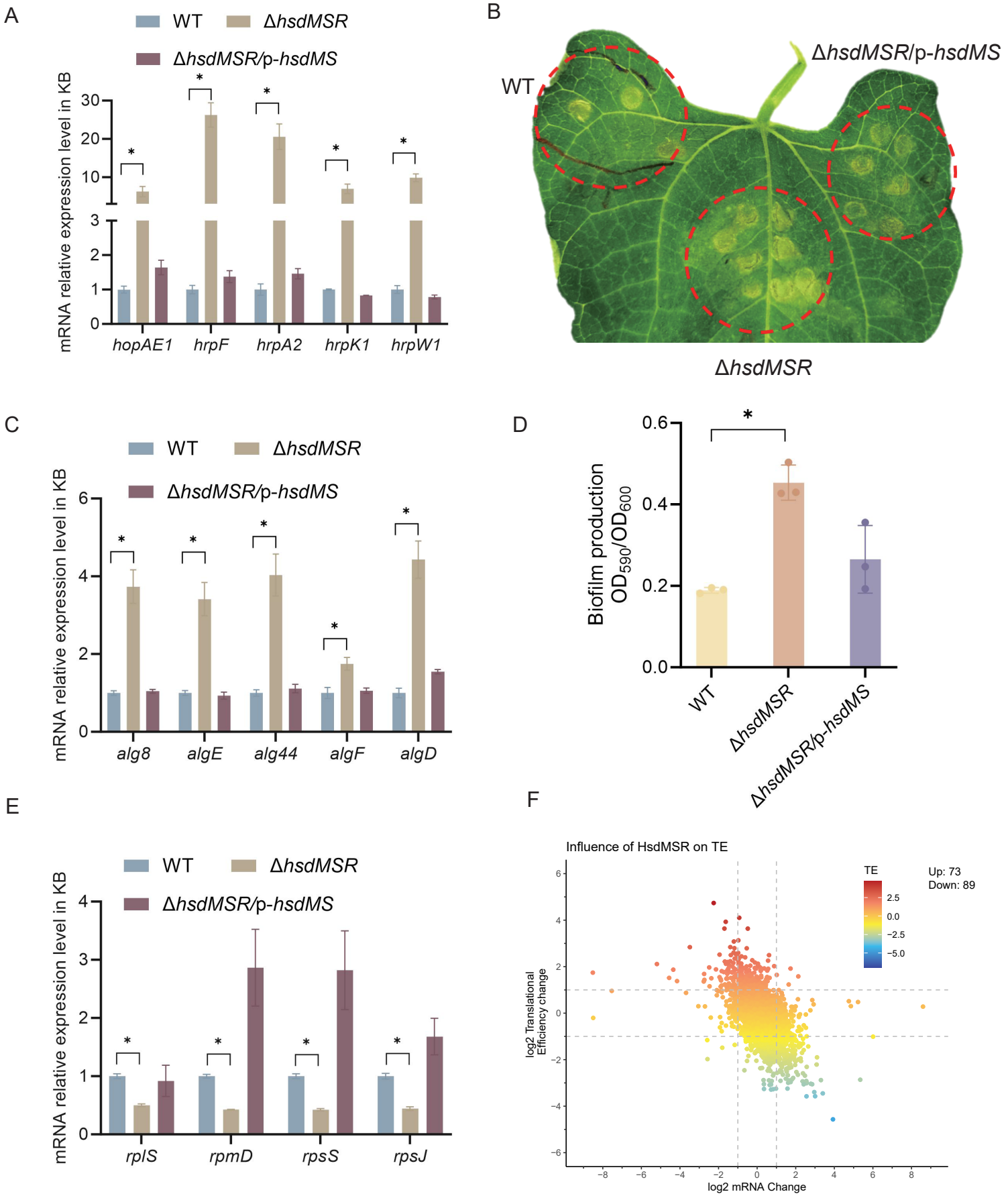
A
WT
ΔhsdMSR
ΔhsdMSR/p-hsdMS
mRNA relative expression level in KB
hopAE1
hrpF
hrpA2
hrpK1
hrpW1
B
WT
ΔhsdMSR/p-hsdMS
ΔhsdMSR
C
WT
ΔhsdMSR
ΔhsdMSR/p-hsdMS
mRNA relative expression level in KB
alg8
algE
alg44
algF
algD
D
Biofilm production
OD590/OD600
WT
ΔhsdMSR
ΔhsdMSR/p-hsdMS
E
WT
ΔhsdMSR
ΔhsdMSR/p-hsdMS
mRNA relative expression level in KB
rplS
rpmD
rpsS
rpsJ
F
Influence of HsdMSR on TE
TE
Up: 73
Down: 89
log2 Translational Efficiency change
log2 mRNA Change

Figure 6

A

B

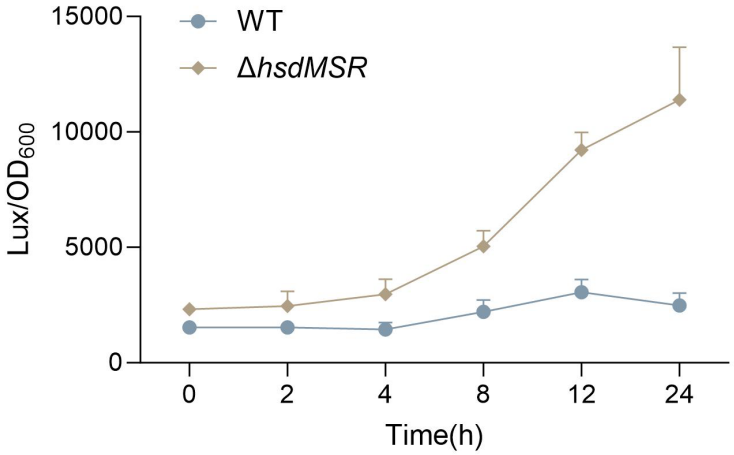

C

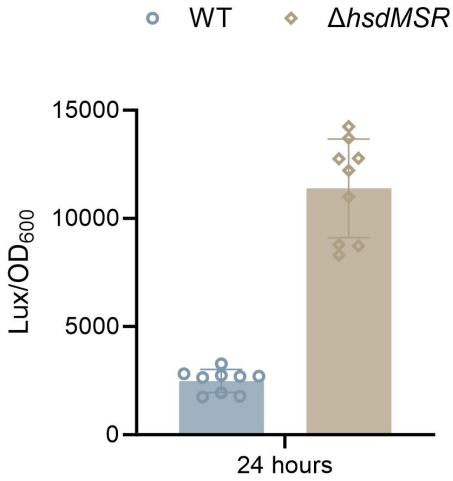

D

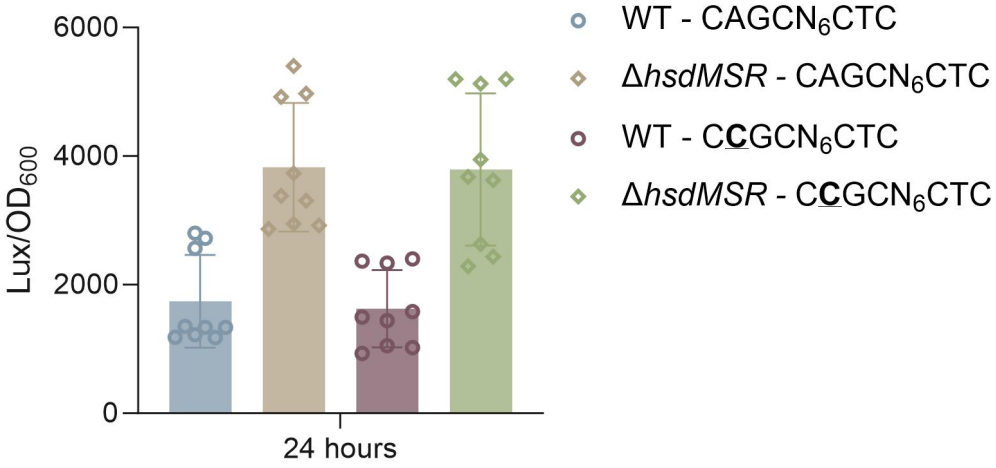
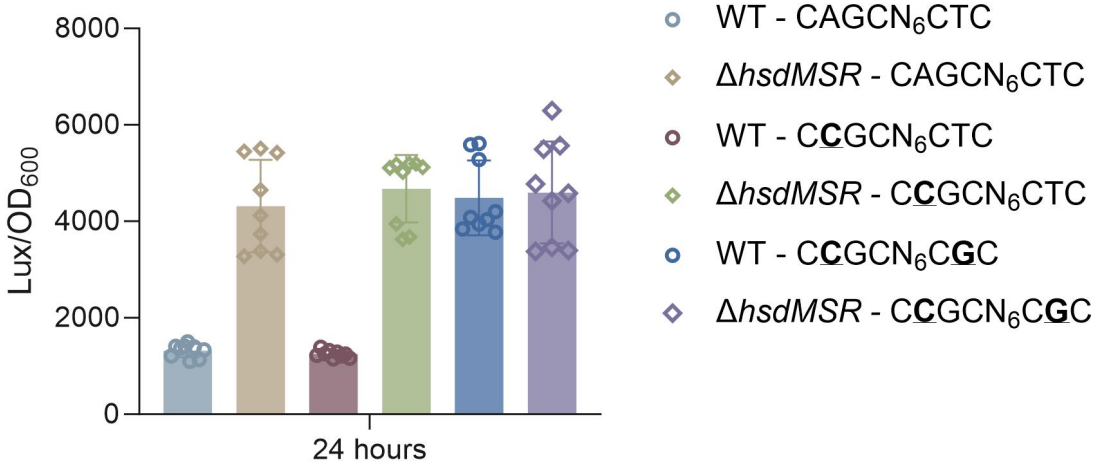
E